FTIR ATR Analysis for Microstructure and Water Uptake in Poly(methyl methacrylate) Spin Cast and Langmuir–Blodgett Thin Films

Peter Sutandar, Dong June Ahn,† and Elias I. Franses*

School of Chemical Engineering, Purdue University, West Lafayette, Indiana 47907-1283

Received February 22, 1994; Revised Manuscript Received August 2, 1994®

ABSTRACT: Spin cast and Langmuir–Blodgett (LB) films of atactic PMMA [poly(methyl methacrylate)] were studied at 25 °C by FTIR ATR (Fourier transform infrared spectroscopy, attenuated total reflection) spectroscopy before and after annealing at 140 °C and after contact with water vapor or liquid. The dichroic ratios of the carbonyl groups revealed that the average molecular orientations of the films remained unchanged upon annealing and also upon exposure to water. However, annealing helped avoiding cracks which appeared in the nonannealed film after contacting liquid water. The absorbances of individual water bands (of the non-hydrogen-bonded monomers, hydrogen-bonded dimers, larger clusters, and associated chains of water) were determined by detailed spectral analysis and compared with a one-dimensional Fickian model. The absorbance data for the annealed spin cast film of thickness of 5.4 μm showed poor fit to the one-dimensional Fickian diffusion model, but the apparent diffusion coefficient, D_{app}, ranged from 5×10^{-10} to 4×10^{-11} cm^2/s. The process of film hydration was found to precede the transfer of bulklike water. For the annealed LB and spin cast films of thickness of 0.1 μm, D_{app} ranged between 10^{-13} and 10^{-15} cm^2/s. It was estimated from ATR carbonyl band intensities that the thin films were about 44% more dense than the thick film, indicating that they had a tighter structure with fewer structural defects or voids. Having more hydrophobic and less rough surface, the LB film showed a longer initial delay in liquid water transport than the spin cast film of the same thickness.

Introduction

Thin PMMA [poly (methyl methacrylate)] films have been studied extensively in the past 15 years for their potential applications as materials for barriers, membranes, microlithography, and optical applications.[1–5] Because controlling the film quality is important for these applications, many workers have reported on the use of various microscopic and spectroscopic techniques for probing pinholes, defects, grain boundaries, etc.[1–5] Important characteristics of quality are the porosity and the permeability of the films to water and other vapors or liquids.

Several techniques have been developed for studying the water transport in PMMA films. In most cases, the sorption kinetics and volumetric changes of PMMA were determined by measuring the weight of the water uptake. Turner reported that sorption dynamics departed from Fick's law.[6] IR and NMR spectroscopy have been used to probe the diffusion of water in polymers.[7–9] Davydov et al.[10] studied the permeability of polyurethane film with respect to water vapor by infrared spectroscopy. Grinsted et al.[11] used NMR imaging to study the sorption–desorption cycle of water and methanol into PMMA rods. Kuan et al.[4,5] reported that spin cast films of PMMA have considerably higher pinhole densities than the LB films. Water transport depends of course on the film quality. Little attention has been given, however, on how the processing method affects the microstructure and the transport properties of these thin films.[7,12]

This article focuses on the FTIR ATR analysis of thin PMMA films made by spin casting or by LB deposition, to obtain a realistic comparison of the two methods. The FTIR ATR spectroscopy is an excellent tool for quantitatively analyzing the microstructural features of dry and wetted films, estimating the water content, and for probing the transport rate of water through the films. This approach can also be useful for studying other penetrants transported through organic thin films.

Two different film thicknesses were produced for studying their differences in regard to the film microstructure, water uptake, and water content. Because microfiltration or ultrafiltration membranes can range from about 1 to 20 μm in thickness,[13] films of about 5 μm were prepared by the spin casting method for evaluating the performance of this polymer as a membrane. By using thick films, one can reduce the IR water signal at the initial measurements after liquid water is placed on top of the film, because the decaying evanescent electric field of the IR beam cannot probe the water on top of the film, but can probe the water in the film. Thus, for thick films one can observe only the transient water uptake, and for thin films one also observes the water on top of the film. Thinner films, of thickness $l = 0.1$ μm, were prepared by the LB and spin casting methods. For an overall evaluation of the film as either a membrane or a barrier material, the dynamics of the water uptake of these two thin films and the thick films was followed.

Experimental Section

Materials. The atactic poly(methyl methacrylate) was obtained from Eastman Kodak; it was polydisperse with $\overline{M}_w$ = 101 000 and $\overline{M}_n$ = 48 300. Polymer films were cast from a chloroform solution (HPLC grade from Aldrich). All water used (DI) was purified using a Milli-Q 4-bowl system, from Millipore Corp., and had an initial resistivity of 18 MΩ/cm.

Spin Casting. Films were cast on the ATR crystals with a spin coater (Model 1-EC101D-R485, Photo-Resist Spinners, Garland, TX). For producing films of about 5.4 and 0.1 μm thickness, respectively, solutions of 200 and 5 mg/mL in chloroform were applied to the entire surface of the ATR crystals. Spinning for 1 min was done at 1000 and 500 rpm, respectively. All films were dried at room temperature for 1 h before they were examined.

* Author to whom correspondence should be addressed. Phone, (317) 494-4078; FAX, (317) 494-0805.

† Present address: Center for Advanced Materials, Lawrence Berkeley Laboratory, MS66-200, Berkeley, CA 94720.

® Abstract published in *Advance ACS Abstracts,* October 15, 1994.

0024-9297/94/2227-7316$04.50/0

Table 1. Thickness, Carbonyl Group Dichroic Ratios (DR_{ATR}), and Average Carbonyl Tilt Angles for Films of Atactic PMMA

film	thickness (μm)	DR_{ATR} (ν C=O) ($\pm$0.02)			$\bar{\gamma}$ (C=O),[a] after annealing
		before annealing	after annealing	after water contact	
thick spin cast film	5.4	0.76	0.76	0.76	65°
thin spin cast film	0.11	0.81	0.82	0.82	50°
thin LB film	0.10	0.82	0.82	0.82	50°

[a] $\bar{\gamma}$ was determined from Figure 2 for thick or thin films.

LB Deposition. The Langmuir trough used to build LB films was a KSV minitrough. The trough used a platinum plate for measuring surface tension and two Teflon barriers for film containment. The trough was housed in a clean room containing a laminar flow hood. The subphase used in the trough was DI water with pH $\approx$ 5.5. PMMA was spread at air/water interface from chloroform solution (0.5 mg/mL). Monolayers of PMMA were deposited on a hydrophilic Si surface under the following LB conditions:[14] 10 min were allowed for solvent evaporation after spreading; 30 min after reaching the desired surface pressure (15 mN/m) were allowed for equilibration. The first monolayer of PMMA was transferred on a hydrophilic Si ATR plate by initially pulling the plate out of the subphase at a speed at 4 mm/min. The first PMMA monolayer was then annealed at about 120 °C for 1 h, for the film to adhere better (otherwise it may peel off). After annealing, the remaining layers were deposited with the same surface pressure and dipping speed. A delay time of 5 min used every time the plate was completely pulled out of the subphase, in order to avoid film peeling off during the subsequent downstroke. With this method it was possible to produce 0.1 μm thick multilayer LB films, after 63 upward and downward strokes (about 15 Å per stroke). Monolayer transfer was initially a Z-type deposition mode (on the way up) for several cycles and then it changed to Y-type deposition (both ways).

Profilometry. After removal of the water, the thickness and the surface roughness of the film were determined by using a profilometer (Alpha-Step 200, Tencor Instrument). A part of the film was removed with methylene chloride, for determining the thickness from the distance between the upper surface of the film and the ATR crystal surface.

Water Vapor Sorption. To study the effect of water vapor sorption for the thicker spin cast films, a film was placed for 3 days in a closed glass container with water vapor coming from a 15 wt % solution of NaCl. This solution lowers the water activity to 0.89 (89% relative humidity),[15] which is important to prevent vapor condensation due to room temperature fluctuations. For calibration purposes, 1.03 g of bulk PMMA was also exposed under the same experimental conditions. The film was equilibrated with vapor along with this bulk sample, which was weighed periodically until a constant weight was achieved, after 1 day normally. A similar experiment with a bulk sample and a water activity of 0.96 was done (using a 6.6 wt % aqueous NaCl solution).

Differential Scanning Calorimetry. Thermograms were obtained with a DuPont DSC-2910 calorimeter, which was equipped with a refrigeration compartment cooled with liquid nitrogen. All thermograms were determined with heating and cooling rates of 5 °C/min. Samples were first cooled to −120 °C, to better ensure that hydration water was frozen. Bulk PMMA (500 mg) with 20 mL of water was filtered through a paper filter, and 10 mg of this wet material was used.

FTIR. The Nicolet 800 FTIR spectrometer was equipped with an internal, computer-controlled, wire grid polarizer. For water vapor and carbon dioxide in the sample chamber to be reduced, the instrument was continually purged with dry air from a Balston air purifier. The ATR optics were custom-built by Connecticut Instrument Inc. The ATR plate was Si (1 × 10 × 50 mm, 45° trapezoid) purchased from Wilmad Glass Co. This plate has a wavenumber cutoff of about 1450 cm^{-1}. An MCT-A detector cooled with liquid nitrogen was used to collect the spectra.

Before various background spectra were collected, the Si ATR plate had been cleaned by sonication at 23 °C in ethanol, trichloroethylene, methylene chloride, ethanol, and DI water, respectively, with 10 min for each step. The treatment was followed by drying in an air jet until no trace of water was observed and then by cleaning in a Harrick Scientific PDC-3XG vacuum plasma cleaner/sterilizer for 15 min.

To observe changes in the film microstructure, background spectra of unpolarized or s- and p-polarized incident beams, with a resolution of 4 cm^{-1} and 256 scans, were collected before the film was formed on the ATR plate. An additional non-polarized background spectrum with a resolution of 8 cm^{-1} and 256 scans was collected for analyzing the spectra (normally with 8 cm^{-1} and eight scans) during the water permeation in the film. All the spectra were taken at the same configuration as the background spectra. One set of three spectra of non-, s-, and p-polarizations with a resolution of 4 cm^{-1} and 256 scans was collected at each step of the experiment, unless indicated otherwise.

Before film spectra were taken, the bottom and the sides of the trapezoid ATR plate were cleaned with methylene chloride. It is important to remove this portion of the PMMA film, in order to enhance the sensitivity of the experiment by observing only the transport in the film on the upper surface. For the effect of annealing to be examined, the films were heated at 140 °C for 1 h in a vacuum oven (at ca. 10^{-4} Torr) and then cooled at room temperature by leaving the sample open to the atmosphere for 1 h. Annealing the film causes the polymer to relax and may produce a much better film with fewer pinholes or film defects than the nonannealed one. The spectra of the film were taken within 1 h after the film had been cooled to room temperature.

The equilibrated water-vapor-sorbed films were removed from the sorption container and immediately enclosed in a sample container which fit on the ATR top crystal surface. This procedure minimized the water vapor desorption from the film during transfer or in the dry air in the FTIR chamber.

For studying the liquid water uptake in the film, liquid water was placed onto the dry films, which were covered, and IR spectra were collected at short time intervals to follow the dynamics of the water permeation within the film. The films were first dried in vacuo at room temperature for 1 h. For obtaining fast spectra (3 s), eight scans with a resolution of 8 cm^{-1} were used initially.

Results and Discussion

Microstructure of Dry Films. Profilometry. FTIR and profilometry revealed substantial differences between the thick and the thin spin cast films and between the two thin films prepared with the spin cast and the LB methods. The spatially averaged film thicknesses were determined by profilometry and are reported in Table 1. For producing spin cast films of about 5 and 0.1 μm thickness, PMMA solutions of 200 and 5 mg/mL in chloroform were cast. Evidently, the thickness of the spin cast film depends mainly on the PMMA concentration and on the rotation speed of the spin coater, as expected from literature correlations.[16] In fact, the predicted thicknesses were quite close to the observed ones, 6 and 0.07 μm. For comparison, only LB films of 0.1 μm thickness were built. Since it takes about one day to build an LB film of 0.1 μm thickness, it may be impractical to build an LB film of 5 μm. The films produced with both deposition methods were visually

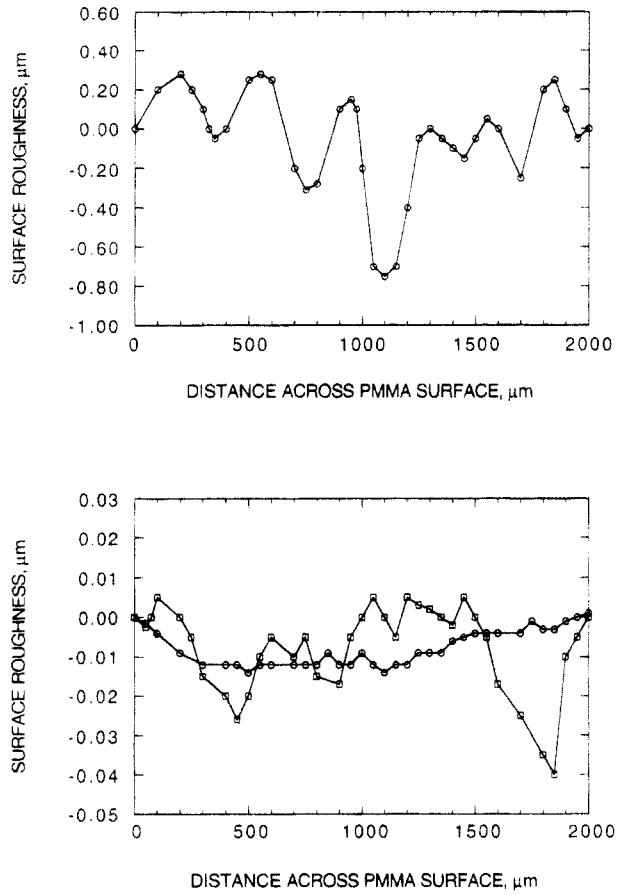

Figure 1. Surface roughness of spin cast atactic PMMA films with thicknesses of 5.4 μm (top, ○) and 0.1 μm (bottom, ○) on a Si crystal using profilometry; also shown are results of LB films (bottom, □).

uniform and bluish, with certain interference fringes observable in the thin spin cast films.

Figure 1 shows the surface roughness of the PMMA films measured along the crystal length from the center. The roughness, from a local maximum to a local minimum, for the thick PMMA film (l = 5.4 μm) was lower than 0.9 μm, or about 17% of the average thickness. For the two thin films, the LB film thickness was more uniform than that of the spin cast film and exhibited a surface roughness of less than 0.01 μm. The thin spin cast film showed a higher surface roughness, ranging from 0.01 to 0.04 μm (or 10 to 40% of the average thickness).

Orientation and Density by FTIR ATR. By measuring dichroic ratios, one can determine whether the orientation can be described by uniaxial, biaxial, or more general distribution functions.[14,17] The dichroic ratio is defined as the ratio of the absorbance intensity (or integrated absorbance) of s-polarized light (electric field normal to the incident plane) to that of p-polarized light (electric field parallel to the incidence plane or TE wave).[8,9] The dichroic ratios of the ν C=O bands were determined from the integrated intensities at each polarization between 1780 and 1670 cm^{-1}.

Recently, it was reported that for the IR transmission mode the dichroic ratios of the ν C=O band for some thin atactic PMMA, for both spin cast and LB films, were close to unity.[14] This indicates that the ν C=O groups are uniaxially oriented on the ATR plates. When the group axes are uniaxially oriented around the surface normal, the group axes have only a preferred tilt angle γ_0. Because the absorbance depends on the inner product of the electric vector of the polarized incident beam and the transition dipole moment, the dichroic ratio for uniaxial orientation configurations has been derived for transition moments parallel to the molecular chain axis ($\Theta = 0°$, where Θ is the angle between the chain axis, if it can be defined, and the dipole moment) as[14,17]

$$\mathrm{DR}(\gamma_0; \Theta = 0°) = \frac{E_y^2 \sin^2\gamma_0}{E_x^2 \sin^2 \gamma_0 + 2E_z^2 \cos^2 \gamma_0} \quad (1)$$

and for perpendicular transition moment ($\Theta = 90°$) as

$$\mathrm{DR}(\gamma_0; \Theta = 90°) = \frac{E_y^2(\cos^2 \gamma_0 + 1)}{E_x^2(\cos^2\gamma_0 + 1) + 2E_z^2 \sin^2 \gamma_0} \quad (2)$$

The electric field amplitude functions at the ATR plate/film interface (at the film side), E_x^2, E_y^2, and E_z^2, depend upon the incident angle of the IR beam and the refractive indexes of the substrate, film, and the ambient gas. Harrick[8] and Haller and Rice[18] have reported analytical expressions for the above functions E_i^2 for a film with a refractive index n_2 on an ATR plate with index n_1, surrounded by an ambient gas with index n_3 (the three-phase problem). The approximate penetration depth, d_p, of the evanescent wave through the film is defined as

$$d_p \equiv \frac{\lambda}{2\pi n_1(\sin^2\theta_i - n_{21}^2)^{1/2}} \quad (3)$$

where λ indicates the wavelength of the IR beam (in vacuo) and θ_i indicates the angle of incidence (here, θ_i = 45°); n_{ij} is a refractive index ratio, i.e., $n_{ij} = n_i/n_j$. When the film thickness, l, is much smaller than the penetration depth ($l \ll d_p$) the amplitude functions are as follows:

$$E_x^2 = \frac{4\cos^2\theta_i(\sin^2\theta_i - n_{31}^2)}{(1 - n_{31}^2)\{(1 + n_{31}^2)\sin^2\theta_i - n_{31}^2\}} \quad (4)$$

$$E_y^2 = \frac{4\cos^2\theta_i}{1 - n_{31}^2} \quad (5)$$

$$E_z^2 = \frac{4\cos^2\theta_i \sin^2\theta_i n_{32}^4}{(1 - n_{31}^2)\{(1 + n_{31}^2)\sin^2\theta_i - n_{31}^2\}} \quad (6)$$

If $l \gg d_p$, for thick films (two-phase system), then E_x^2 and E_y^2 are given by the above formulae, but with n_{32} being replaced by n_{21}. Moreover, E_z^2 is given by the following equation:

$$E_z^2 = \frac{4\cos^2\theta_i \sin^2\theta_i}{(1 - n_{21}^2)\{(1 + n_{21}^2)\sin^2\theta_i - n_{21}^2\}} \quad (7)$$

No simple equation is available at present for intermediate layer thicknesses ($l \approx d_p$).

Equations 4–7 were developed originally for weakly absorbing films,[8,19] but are practically valid for a wide range of extinction coefficients of the film (k_2), as shown by Harrick and Carlson.[20] For example, when n_1 = 4.0, n_2 = 1.5, n_3 = 1.0, and θ_i = 45°, the simple equations are adequate for $k_2 \leq 0.5$ for thick films and $k_2 \leq 1.5$ for thin films.[20] For PMMA, the extinction coefficient is less than 0.05 for the CH stretching bands and about

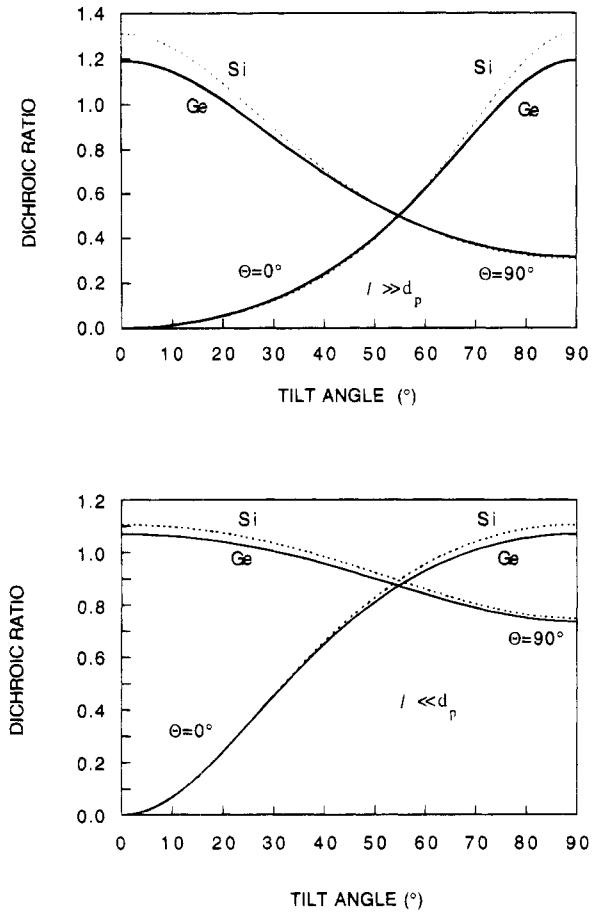

Figure 2. ATR dichroic ratios for uniaxial orientation distributions of chains or transition moments for film thickness $l \gg d_p$ (top) and $l \ll d_p$ (bottom); for $\Theta = 90°$, the abscissa is the angle between the chain axis and the surface normal; for $\Theta = 0°$, the abscissa is the angle between the transition moment and the surface normal (see ref 17 for details); substrates are Ge ($n_1 = 4.03$) and Si ($n_1 = 3.42$); $n_2 = 1.5$ (film) and $n_3 = 1.0$ (ambient gas).

0.4 for the C=O stretching band.[21,22] For the water OH stretching band at 25 °C, it is ca. 0.3.[23] By using eqs 1, 2, and 4–7, one can determine the dichroic ratio as a function of the tilt angle, γ_0, for a uniaxial distribution of molecular chain axes (Figure 2). The film thickness, l, is clearly an important parameter of the ATR dichroic ratios. The dichroic ratio for the so-called "magic angle" is equal to that for a totally randomly oriented molecular orientation.[17] When the tilt angle equals the magic angle, at 54.7°, the dichroic ratio is 0.5 for thick films (for both the Si and the Ge plates). For the thin film regime, the dichroic ratios are 0.87 and 0.89 for Ge and Si plates, respectively. If the tilt angles are distributed with an average value of $\bar{\gamma}$, then $\bar{\gamma}$ is determined.

One can use FTIR absorbances for estimating the film density as follows. The integrated absorbance of a certain band of an isotropic film can be expressed as:[24–26]

$$A_j^I = \int_0^l \varrho_f \alpha_f e^{-2\gamma_f x}\, dx = \frac{\varrho_f \alpha_f}{2\gamma_f}(1 - e^{-2\gamma_f l}) \qquad (8)$$

Here ϱ_f, α_f, and γ_f are the film density, specific absorptivity, and inverse penetration depth ($\equiv d_p^{-1}$) of the film, respectively. As indicated by the above equation, the integrated absorbance has an asymptotic value of A_j^I as l becomes larger than $(2\gamma_f)^{-1}$. This case is denoted by "$l \to \infty$". Thus, one can determine α_f by estimating

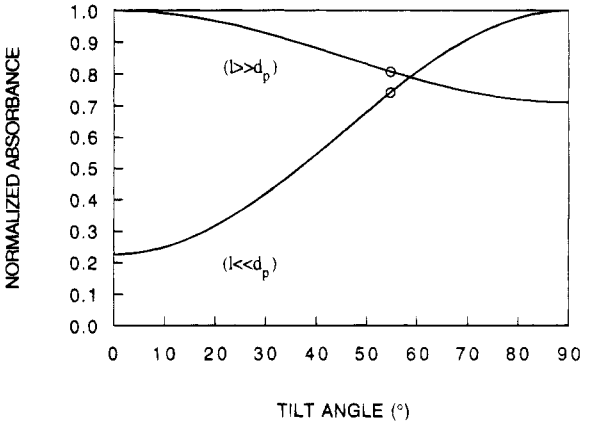

Figure 3. Normalized absorbance (for unpolarized light) for thick and thin films with $\Theta = 0°$. Circles indicate the magic angle for the thickness regime (54.7°). Calculations were done with $n_1 = 3.42$ (Si), $n_2 = 1.5$, and $n_3 = 1.0$; see text for details.

the integrated absorbance of a certain band from a thicker film as follows:

$$\alpha_f = \frac{2\gamma_f A_j^I(l \to \infty)}{\varrho_{thick}} \qquad (9)$$

With eqs 8 and 9 and the value of γ_f based on the ν C=O band, the integrated absorbance of the thin film can be determined. Moreover, since the thickness can be independently measured by profilometry, the density ratio $\varrho_f/\varrho_{thick}$ can be estimated to the first order. Since these equations were derived for an isotropic film, usually a small correction has to be made on these absorbances for films which have a preferred tilt angle, γ_0. Figure 3 shows how these absorbances change with tilt angle and can form the basis for this correction. For an isotropic film, one has to calculate the absorbance with respect to the magic angle at 54.7°. Hence, by using an ATR dichroic ratio of the ν C=O absorbance and its tilt angle for thin or thick films (from Figure 2), one can obtain the corrected ν C=O absorbance for its corresponding isotropic film from Figure 3.

Polarized and nonpolarized spectra with 256 scans and a resolution of 4 cm^{-1} were collected for each film to probe for structural changes within the film. Figure 4 shows the nonpolarized spectra of the thick spin cast film before and after annealing. The spectrum of the thin spin cast film is qualitatively similar, but of course with lower peak intensities. Peak assignments for PMMA films are given in Table 2.[27,28] Since after film annealing the shoulder peak between 3000 and 3100 cm^{-1} disappears, it could be assigned to the chloroform C–H stretch band.[29] The rest of the spectrum remains the same. The peak change is probably due to annealing causing the polymer to relax, allowing some remaining chloroform traces in the film to escape from the film.

The band between 1780 and 1670 cm^{-1} on the polarized spectra was integrated, for determining the dichroic ratio of the ν C=O band. Since for polymer films one cannot define a linear chain axis, the molecular orientation for such a system can be described only from the group dipole moment, i.e. by setting $\Theta = 0°$.[17] The average tilt angle, $\bar{\gamma}$, of a specific transition moment can then be determined for spin cast and LB films from the dichroic ratio of ν C=O, as given in Table 1. This angle provides a measure of the overall orientation in the film. Surprisingly, the dichroic ratio, D, of the ν C=O band was the same for each film before and after the annealing procedure. For the thick spin cast film,

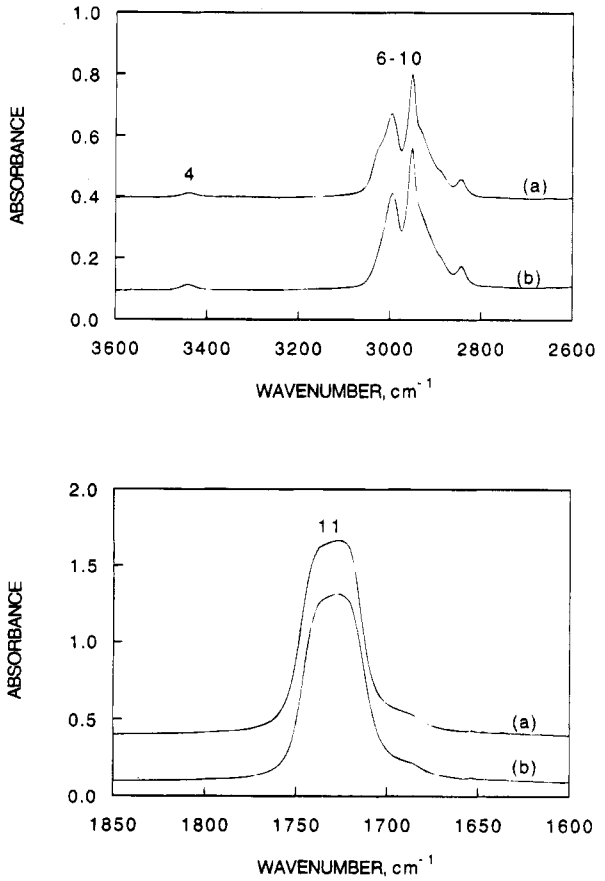

Figure 4. FTIR ATR spectra of spin cast atactic PMMA film with thickness of 5.4 μm before annealing (a) and after annealing (b); unpolarized light was used; see Table 2 for peak assignments.

Table 2. IR Band Peak Assignments for Atactic PMMA (see Figures 4–6)[a]

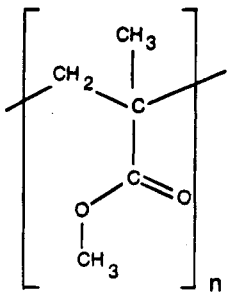

peak	assignment
1	water peak[a]
2	water peak[a]
3	water peak[a]
4	overtone of ν C=O
5	water peak[a]
6	ν_a CH_3–O
7	ν_a CH_3–C
8	ν_s CH_3–O
9	ν_a CH_2
10	ν_s CH_3–C, ν_s CH_2
11	ν C=O
12	b (s) OH

[a] Water peaks will be discussed in certain spectra later (after contact of PMMA with water).

D was 0.76. One can then use eq 1 or Figure 2 (top) to determine the angle of the carbonyl group axis when $\bar{\gamma}$ = 65°. The dichroic ratios for thin spin cast and LB films before and after annealing were also the same, 0.82, which corresponds to $\bar{\gamma}$ = 50°. Clearly, there was no effect of annealing on the molecular orientations of the C=O groups. One interesting result was that all the films examined were nonrandomly oriented, even though the films consisted of atactic PMMA, were annealed, and were not stretched. For the thick film, the dichroic ratio differed by 0.26 from that expected for a randomly oriented film. By contrast, the dichroic ratios for both thin films were lower by only 0.07 from the value expected for a random film. Other evidence that the carbonyl groups in similar thin films can be oriented comes from a surface potential study.[30] Apparently, the film formation mechanism should cause some orientation. This suggests that there may be a strong interaction between the Si substrate and the C=O groups of the polymer chains as they precipitate from solution. The identical dichroic ratios of the thin films also indicate that the molecular orientation depends less on the processing method and more on the effects of the substrate/PMMA interactions.

Polarized and nonpolarized spectra of the films were also taken after the water was removed at the end of the water uptake environment. No change was observed in the intensity of the ν C=O band for each film, or in the dichroic ratio of this band (Table 1), implying that there was neither significant swelling of the material nor orientation change of the transition moment of the ν C=O band. The intensities and dichroic ratios of the hydrocarbon bands 6 and 7 were determined. No significant changes were detected in the dichroic ratios, being 0.66 and 0.65, respectively, before water contact and 0.67 and 0.64 after water contact. The dichroic ratios for band 6 for the thin films showed no significant change, being 0.85 and 0.81, before water contact and 0.83 and 0.78 after water contact for the LB and the spin cast films, respectively. Similarly, the dichroic ratios of band 7 of the LB film showed little, if any, change, from 0.54 to 0.56. There was, however, a considerable change on the dichroic ratio for band 7 of the thin spin cast film, from 0.54 to 0.79, indicating that upon water contact there was some orientation change, and hence some mobility of the CH_3C groups.

The density ratio $\varrho_f/\varrho_{thick}$ was estimated from integration of the ν C=O band, yielding an absorbance (for unpolarized light) of 22.6 cm^{-1} for the thin spin cast and the LB films and 47.9 cm^{-1} for the thick films. These absorbances (for the oriented films) were corrected to corresponding values for isotropic films, by the use of the tilt angles (from Table 1) and Figure 3. The corrected absorbances were found to be 24.8 and 50.7 cm^{-1} for the thin and thick films, respectively. The density ratio was 1.44, suggesting that the thin films were more dense than the thick film.

IR Spectral Analysis. For better determining the areas of the overlapping peaks, the spectra between 4000 and 2600 cm^{-1} were deconvoluted. The best fits at a 95% confidence level were obtained for Figure 5 with peaks being 50% Lorentzian and 50% Gaussian. The peak assignments and the curve fit parameters are listed in Tables 2 and 3. Figure 5 reveals six fundamental peaks in this region. Band 4 is clearly visible in the water region, but its location does not correspond to any OH vibration. This peak is due to the overtone of the ν C=O stretch at 1750 cm^{-1} (peak 11; see Figure 3). The position and line width (FWHM) for band 4 were determined from the spectral analysis of the film and were set constant for the other spectral analyses. The bands between 3200 and 2600 cm^{-1} are due to the

Table 3. IR Parameters for Atactic PMMA Films after Annealing (Figure 5)

film	peak	position (±1 cm^{-1})	peak intensity	FWHM[a] (cm^{-1})	area (cm^{-1})	area relative to area of peak 6
thick spin	4	3452	0.022	73	2.1	12
cast	6	3012	0.29	46	17	100
	7	2969	0.35	20	9.4	55
	8	2947	0.13	30	5.1	30
	9	2923	0.11	58	8.5	50
	10	2861	0.053	23	1.6	9.4
thin spin	4	3451	0.0064	42	0.29	5.2
cast	6	3012	0.10	42	5.6	100
	7	2969	0.13	21	3.7	66
	8	2942	0.072	38	3.6	64
	9	2906	0.020	35	0.90	16
	10	2865	0.022	22	0.63	11
LB	4	3452	0.0058	42	0.26	4.6
	6	3012	0.099	43	5.6	100
	7	2969	0.13	21	3.5	63
	8	2942	0.073	38	3.6	64
	9	2907	0.019	35	0.90	16
	10	2865	0.021	22	0.60	11

[a] FWHM ≡ full width at half maximum.

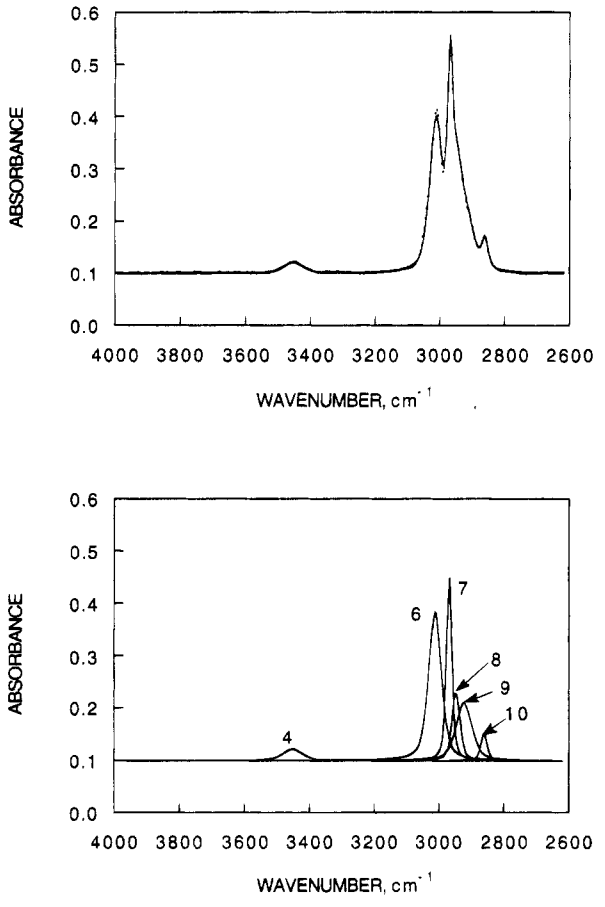

Figure 5. Spectral analysis of CH stretch region for spin cast atactic PMMA annealed film (Figure 2, top, b). In the top, the dots are the actual spectrum and the line is the fit. The individual peaks are shown at the bottom; see Tables 2 and 3 for peak assignments and curve fit parameters.

CH stretching vibrations. No significant differences were observed in the relative areas for the thin spin cast and LB films (Table 3). Consequently, the thin spin cast and the LB films had a similar group orientation for all hydrocarbon bands. The different relative areas and the line widths in the thick spin cast film suggest that the thick film had a different molecular orientation from that of the thin films. The difference is probably due to the different adsorption conditions of the polymer on the substrate and possibly different shear deformation of the polymer chains during the spinning process.

Films with Sorbed Water Vapor. Motivation. The primary purpose of this experiment is to investigate the water vapor sorption and to estimate the hydration water content in the thick spin cast film. This information is important, for directly linking these results to the results of the liquid water uptake in the film and for determining the quality of the film as a vapor barrier. Although the film was in contact with only water vapor of a relative humidity of 89%, results showed that bulklike water was still present in the film. Apparently, the hydration water in the film, monitored from the OH stretch vibration, consists of both non-hydrogen-bonded and hydrogen-bonded components. The relative areas of the hydrocarbon region were also compared, for determining the effect of water vapor sorption in the film microstructure.

Vapor Sorption Data. For calibration of the IR intensities, one needs to independently determine the content of water sorbed in the film. Since thin films contain only a small (and hard to weigh precisely) amount of sorbed water vapor, one may use bulk PMMA to determine the content of hydration water gravimetrically, assuming that the capacity of bulk PMMA for water vapor sorption is the same as that of the film. Bulk PMMA and thick spin cast films were exposed to water vapor in the same vessel. The density of the sorbed water at 89 and 96% relative humidity in the equilibrated bulk PMMA were, respectively, 0.017 and 0.023 g/cm^3 (g of water per cm^3 of polymer). These latter densities were used to linearly extrapolate the result for 100% relative humidity (which is necessary for estimating the content of sorbed water in the thick film upon contact with liquid water) as 0.027 g/cm^3.

FTIR Results. Figure 6 shows the spectrum of the equilibrated thick film. The broad bands of the OH stretching region between 3800 and 3100 cm^{-1} and the OH deformation (Band 12) between 1650 and 1600 cm^{-1} are observed. To analyze the water spectrum quantitatively, the first broad band was deconvoluted into five peaks: four peaks due to water and an additional peak due to the overtone of the ν C=O band. The best fit was obtained when the former four peaks were pure Gaussian and the latter peak was 50% Gaussian and 50% Lorentzian. These parameters were also used to deconvolute this band in later experiments. The peak assignments and curve fit parameters are given in Tables 2 and 4, respectively.

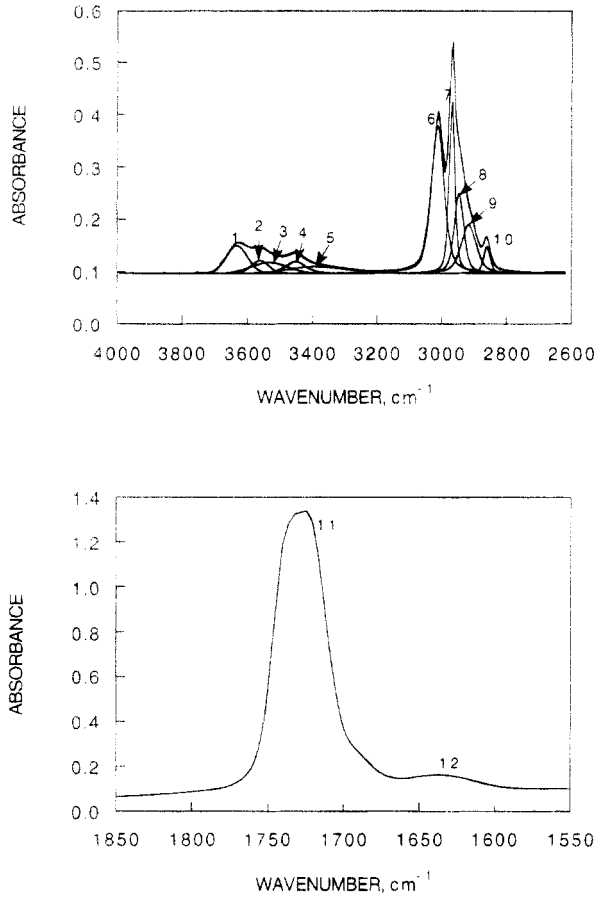

Figure 6. Spectral analysis (top) for an annealed spin cast atactic PMMA film (of thickness 5.4 μm), which was exposed at 23 °C to water vapor with relative humidity of 89%; the solid line is the overall fit; the actual spectrum overlaps with the overall fit; see Table 4 for curve fit parameters; also shown is the spectral region showing the C=O stretch band and the water bend deformation band; unpolarized light was used.

Table 4. IR Parameters for Thick PMMA Film after Exposure to Water Vapor[a] for 3 Days (Figure 6)

peak	position (±1 cm^{-1})	peak intensity	FWHM (cm^{-1})	area (cm^{-1})	area relative to area of peak 6
1	3632	0.052	75	4.2	25
2	3561	0.024	64	1.7	10
3	3534	0.021	127	2.8	16
4	3452	0.022	73	2.1	12
5	3382	0.013	203	2.8	16
6	3013	0.28	46	17	100
7	2969	0.33	21	9.0	53
8	2947	0.15	34	6.9	41
9	2918	0.093	55	6.7	39
10	2861	0.052	23	1.6	9.4

[a] The water activity was 0.89.

The FTIR spectrum of bulk liquid water on the ATR crystal (with no film) is shown in Figure 7. The curve fit parameters are given in Table 5. Band 1 (centered at 3616 cm^{-1} with FWHM of 83 cm^{-1}) corresponds to monomeric non-hydrogen-bonded water (or matrix-isolated dimers).[31-34] It is present in bulk water at 25 °C in proportion of about 3%. Band 2 stems from hydrogen-bonded dimers and band 3 from small hydrogen-bonded clusters. Certain authors (for water-in-oil microemulsions of AOT (or AeroSolOT or sodium bis(2-ethylhexyl) sulfosuccinate[33,34]) have used one combined band instead of our bands 2 and 3. This combination does not alter significantly the conclusions. Finally, band 5 corresponds to a wide distribution of hydrogen-stretch vibration energies in associated chains in water.

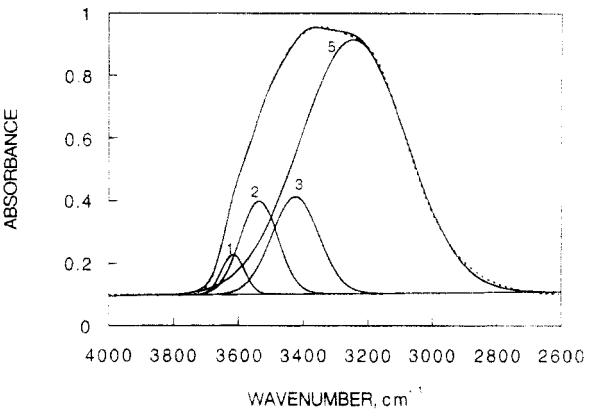

Figure 7. Spectral analysis for bulk water; unpolarized light was used; see Table 6 for curve fit parameters.

Table 5. IR Parameters for Bulk Water (Figure 7)

peak	position (±1 cm^{-1})	peak intensity	FWHM (cm^{-1})	area (cm^{-1})	area relative to area of peak 5
1	3616	0.13	83	11	3.4
2	3536	0.30	138	44	13
3	3424	0.31	171	57	17
5	3246	0.81	386	334	100

Other authors have fit bulk water ATR data by assigning two separate peaks for our band 5.[31] The reason that several bands are observed for the water vibration is simply that the time scale of the vibration (10^{-14} s) is much smaller than the time scale of hydrogen-bond formation and destruction, which is of the order of 10^{-11}–10^{-10} s.[31,32] It is well-established that hydrogen bonding broadens the OH stretch band and enhances the IR intensity.[31,32] Hence, the actual proportion of water in bands 1–3, relative to band 5, is higher than indicated in Table 5.

If bulklike water is present in a film, then some portion of the intensities of bands 1–3 are due to the bulklike water, as suggested from Table 5. If the relative proportions of these bands are higher than for bulk water, as in the film with sorbed water, then they imply that there is additional water in the film. This additional water must be associated with the polymer structure (absorbed on the polymer polar groups or adsorbed on film defects or surfaces of nanopores). Peak 1 of the hydrated film is due almost entirely (98%) to polymer-associated water (except 16 × 0.034 = 0.5 of the relative area, or about 2% of the total). Furthermore, about 80% of peak 2 and 83% of peak 3 are also due to such water of hydration. The film also contains some bulklike water (peak 5), probably due to water in large clusters, or to capillary condensation in film micropores. Peaks 1–3 and 5 of the film are shifted to higher wavenumbers (and smaller line widths) than those of bulk water, probably because of less intense hydrogen-bonding interactions and stronger interactions with the substrate polymer.

The integrated absorbances of the water peaks can be used to provide a first-order estimate of the water density in the film, based on simple ATR theory.[24] The integrated absorbance of water in the film, A_W^I (in cm^{-1}), can be expressed as follows:[26]

$$A_W^I = \int_0^l \varrho_{wf}\alpha_{wf} e^{-2\gamma_f x}\,dx = \frac{\varrho_{wf}\alpha_{wf}}{2\gamma_f}(1 - e^{-2\gamma_f d}) \quad (10)$$

Here, ϱ_{wf} is the water density in the film, which is presumed to be isotropic and uniform, α_{wf} is the specific absorptivity of water in the film (including Bands 1–3

and possibly 5), l is the film thickness, $\gamma_f = 4.02 \times 10^4$ cm^{-1} when the film refractive index is $n_2 = 1.5$, the Si plate refractive index is $n_1 = 3.42$, and the IR wavelength for the water band is $\lambda = 2.97 \times 10^{-4}$ cm. The integrated absorbance under identical conditions of a thick bulk water layer on the sample plate, A_B^I, can be estimated to be

$$A_B^I = \int_0^\infty \varrho_{ww}\alpha_{ww}e^{-2\gamma_w x}\,dx = \frac{\varrho_{ww}\alpha_{ww}}{2\gamma_w} \qquad (11)$$

where ϱ_{ww} is the bulk water density (1.0 g/cm^3), γ_w is the inverse penetration depth of bulk water ($\equiv d_{pw}^{-1}$), which is 4.27×10^4 cm^{-1} when the water refractive index is $n_2 = 1.33$ and when both n_1 and λ are the same as before. By using the measured value of $A_B^I = 446$ cm^{-1} and eq 11, one can obtain the absorptivity of water in bulk water as $\alpha_{ww} = 3.76 \times 10^7$ cm/g. Combining eqs 10 and 11 yields the following equation:

$$\varrho_{wf} = \varrho_{ww}\frac{A_w^I}{A_B^I}\frac{\alpha_{ww}}{\alpha_{wf}}\frac{\gamma_f}{\gamma_w}\frac{1}{(1 - e^{-2\gamma_f l})} \qquad (12)$$

For $A_W^I = 11.5$ cm^{-1}, $l = 5.4$ μm, and $\alpha_{wf} \cong \alpha_{ww}$, one obtains $\varrho_{wf} = 0.024$ g/cm^3. This is different from the value of 0.017 g/cm^3, determined gravimetrically from the vapor sorption data for the bulk sample. Alternatively, if ϱ_{wf} is assumed to be equal to the density of the sorbed water in the bulk film, it follows that $\alpha_{wf} = 5.53 \times 10^7$ cm/g. Probably, the assumption that $\alpha_{wf} \cong \alpha_{ww}$ is incorrect, because of different hydrogen-bonding interactions in the film, and is a source of error for determining the density of the water sorbed in the film. If precise values of absorptivities of the different water bands become available, improved density estimates may become possible.

There was no significant change in the dichroic ratio of ν C=O band after it has been exposed to water vapor. There was, however, a significant change on the relative area of peaks 8 and 9, from 30 and 50 to 41 and 39, respectively (see Tables 3 and 4). This implies that some conformational or orientational changes occurred on the CH_3O and CH_2 groups when hydration water filled the gaps, holes, or defects in the film. These changes were probably reversed after drying (Table 1).

DSC Results. No melting or freezing peak of the hydration water was observed in the thermogram. This showed either that the technique was not sensitive enough to detect any possible thermal activity of the water or that this water did not freeze. By contrast, the DSC technique did show the usual freezing or melting point of the bulklike water when bulk PMMA was mixed in water and filtered (approximately 50 wt %). Nonbulklike water in this sample was not detected. Possibly the sorbed water (peaks 1–3 and possibly some of peak 5) cannot be frozen because of its close proximity to the polymer molecules and its nonaggregated state. It is not clear why the freezing of water of peak 5 was not observed (if it indeed occurred).

Dynamics of Water Uptake by Thick and Thin Films. Transport Data. We now consider the spectra of the water uptake dynamics. There are two bands of interest: the OH stretching region (between 3800 and 3100 cm^{-1}) and the OH deformation band (between 1650 and 1600 cm^{-1}). These signals gradually increased with time as water was taken up into the film and was probed by the evanescent wave. Since the penetration

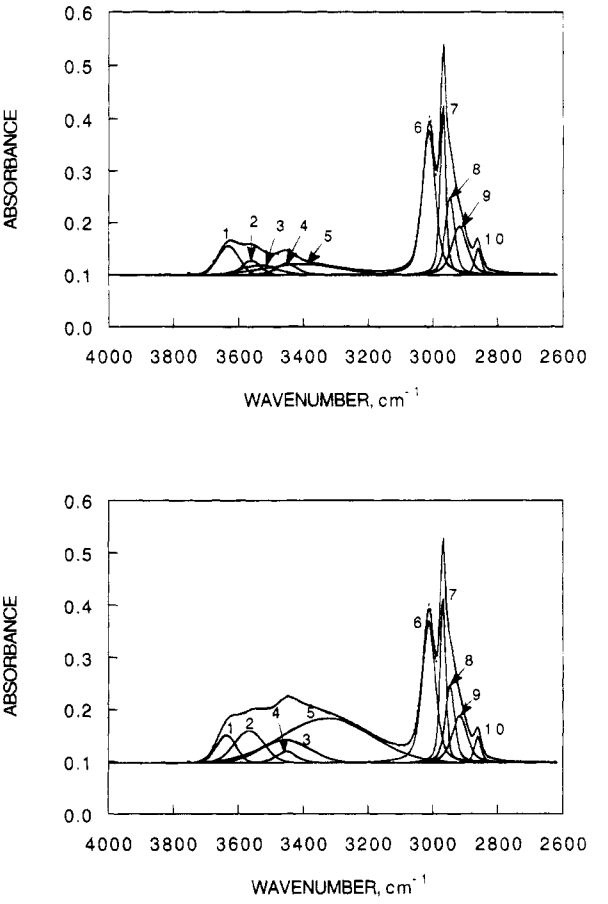

Figure 8. Spectral analysis for an annealed spin cast atactic PMMA film with thickness of 5.4 μm after water contact a $t \cong 3$ s (top) and after equilibration with water at $t \cong 4$ h (bottom); unpolarized light was used; see Table 5 for curve fit parameters.

length of the 1650–1600 cm^{-1} band is approximately twice that of the 3800–3100 cm^{-1} band, a larger fraction of the total water signal, originating from the water on top of the film, may appear in the former band, limiting its use for measuring water transport in the film. Hence, the latter band was used for subsequent analysis.

Spectra were collected for the film at increasing times after water contact. Examples of spectra for the thick spin cast film at an early time and after equilibration are shown in Figure 8. The first spectrum ($t \approx 0$) was obtained within 3 s after the water filled the container above the film. Peaks 1–3 increased faster than the bulklike water (peak 5, centered at 3350 cm^{-1}). The latter band at $t \approx 0$ was larger in this film than in the water-sorbed film and eventually dominated the region between 3800 and 3100 cm^{-1}, as more bulklike water entered the film. Figure 9 shows the time dependence of the absorbances of Peaks 1–3 and 5. The film was apprently saturated with non-hydrogen-bonded water in a much shorter time (25 min) than with bulklike water (~3 h). This indicates that the process of film hydration was completed well before transport of bulklike water stopped.

The thick nonannealed film was also exposed to water under the same conditions as the annealed film. The results were less satisfactory, because the film cracked, and they are reported in the appendix.

The water band of the spectrum (of the annealed film) at $t \approx 3$ s looks identical to that of the spectrum shown in Figure 6. Comparison of the spectral parameters

Table 6. IR Parameters for Thick Spin Cast Film after Contact with Liquid Water (Figure 8)

	peak	position (±1 cm^{-1})	peak intensity	FWHM (cm^{-1})	area (cm^{-1})	area relative to area of peak 6
thick spin	1	3632	0.056	75	4.4	26
cast film	2	3561	0.027	68	1.9	11
at $t \approx 0$ (3 s)	3	3538	0.019	130	2.6	15
	4	3452	0.022	73	2.1	12
	5	3405	0.020	277	6.0	35
	6	3013	0.28	46	17	100
	7	2969	0.33	21	8.9	52
	8	2948	0.15	34	6.7	39
	9	2918	0.094	56	6.9	41
	10	2861	0.051	23	1.6	9.4
thick spin	1	3638	0.054	72	4.1	26
cast film	2	3567	0.062	108	7.1	42
at $t = \infty$ (4 h)	3	3456	0.044	180	8.5	50
	4	3452	0.022	73	2.1	12
	5	3326	0.085	325	30	180
	6	3013	0.27	47	17	100
	7	2969	0.32	20	8.7	51
	8	2948	0.15	34	6.7	39
	9	2917	0.091	55	6.7	39
	10	2861	0.050	24	1.6	9.4

Table 7. IR Parameters for Thin Spin Cast Film after Contact with Water (Figure 10)

	peak	position (±1 cm^{-1})	peak intensity	FWHM (cm^{-1})	area (cm^{-1})	area relative to area of peak 5
thin spin	1	3639	0.090	77	7.3	3
cast film	2	3563	0.22	133	31	13
at $t \approx 0$ ($t = 3$ s)	3	3448	0.21	156	39	16
	4	3452	0.006	42	0.29	0.12
	5	3304	0.66	345	240	100
	6	3014	0.13	45	7.6	3.2
	7	2968	0.18	28	6.7	2.8
	8	2936	0.10	32	4.4	1.8
	9	2903	0.034	36	1.6	0.67
	10	2865	0.036	36	1.7	0.71
thin spin	1	3639	0.098	77	8.0	2.8
cast film	2	3561	0.25	133	35	12
at $t = \infty$ ($t = 1$ h)	3	3444	0.28	156	47	16
	4	3451	0.006	42	0.29	0.12
	5	3300	0.81	332	287	100
	6	3015	0.14	45	8.3	2.9
	7	2968	0.18	28	6.9	2.4
	8	2937	0.11	32	4.5	1.6
	9	2906	0.039	39	2.0	0.69
	10	2865	0.038	38	1.9	0.66

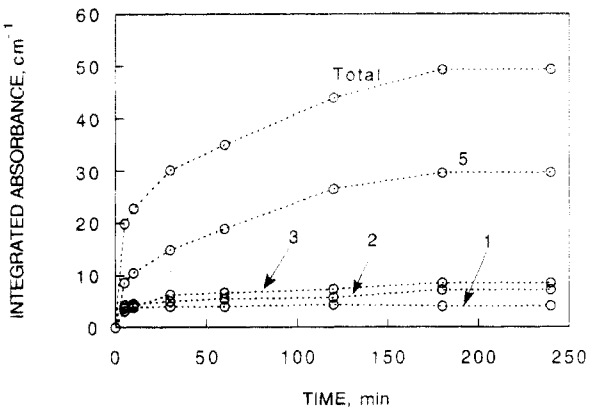

Figure 9. Integrated absorbances of individual water bands 1–3 and 5 and total water absorbance for water penetrating a thick (5.4 μm) annealed spin cast PMMA film.

(Tables 4 and 6) shows that there was a major change only in peak 5. Apparently, as more water was taken up in the film, more bulklike (fully hydrogen bonded) water clusters appeared in the film (see peak 5 in Figure 8). This is consistent with the hypothesis that water transport occurred first via water vapor, before bulk liquid water penetrated or condensed, as smaller clusters or individual molecules should be transported faster than larger clusters. As more water was taken up by the film (see Table 6), the center positions of peaks 3 and 5 shifted to lower wavenumbers by ca. 82 and 79 cm^{-1}, respectively. In addition, larger line widths (FWHM), were observed for peaks 2, 3, and 5 after the film was in contact with water for 4 h. From the relative areas and the line widths in the hydrocarbon region (Tables 4 and 6), it is clear that there were no significant structural differences between the film exposed to water vapor and the film in contact with water at $t \approx 3$ s and at $t \approx 4$ h.

Figures 10 and 11 show examples of spectra collected at 3 s ($t \approx 0$) and after equilibration time ($t = \infty$) for the thin films. A large water peak was observed from the first measurement. This was due partly to the evanescent IR wave extending beyond the thin film/water boundary and interacting with water present on top of the films. By contrast to the thick film results, peaks 1–3 for the thin films were small compared to peak 5, because much more bulklike water on the top of the films was detected (see eqs 13 and 14 below). For convenience, peak 5 (of water) rather than peak 6 (of the polymer), which is small for thin films, was used as the basis for calculating the relative areas of the peaks in the thin films. The saturation times of the spin cast and the LB films were 2 and 4 min, respectively. Peaks 1–3 again reached their steady values well before peak 5, again indicating that bulk liquid water lagged the sorbed water in getting into the film.

Table 8. IR Parameters for LB Film after Contact with Water (Figure 11)

	peak	position (±1 cm^{-1})	peak intensity	FWHM (cm^{-1})	area (cm^{-1})	relative area to area of peak 5
LB film	1	3624	0.091	82	7.9	3.2
at $t \approx 0$ ($t = 3$ s)	2	3534	0.20	137	29	12
	3	3416	0.15	129	20	8.0
	4	3452	0.006	42	0.26	0.10
	5	3297	0.64	368	250	100
	6	(2989)[a]	0.13	20	3.7	1.5
	7	(2945)[a]	0.14	38	6.7	2.7
	8	(2919)[a]	0.070	43	4.0	1.6
	9	(2887)[a]	0.039	48	2.5	1.0
	10	(2836)[a]	0.030	30	1.2	0.48
LB film	1	3625	0.088	78	7.3	2.3
at $t = \infty$ ($t = 1$ h)	2	3535	0.23	143	34	11
	3	3413	0.17	130	22	7.0
	4	3452	0.006	42	0.26	0.08
	5	3303	0.80	363	314	100
	6	(2989)[a]	0.14	21	3.7	1.2
	7	(2949)[a]	0.11	38	5.5	1.8
	8	(2922)[a]	0.11	43	4.4	1.4
	9	(2882)[a]	0.033	36	1.6	0.51
	10	(2838)[a]	0.026	28	0.95	0.30

[a] These frequencies were different from the LB film without water and from similar results for thin spin cast film. They are considered unreliable because of poor fit (Figure 11). The poor fit is probably due to the large water peaks and the baseline noise.

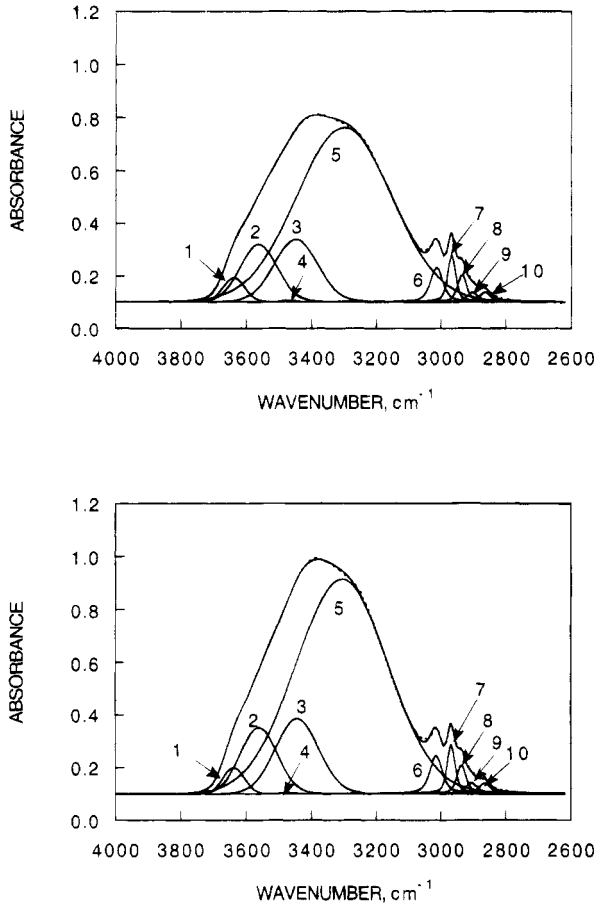

Figure 10. Spectral analysis for an annealed spin cast PMMA film with thickness of 0.1 μm after water contact at $t \cong 3$ s (top) and after equilibration with water at $t \cong 1$ h (bottom); unpolarized light was used; see Table 7 for curve fit parameters.

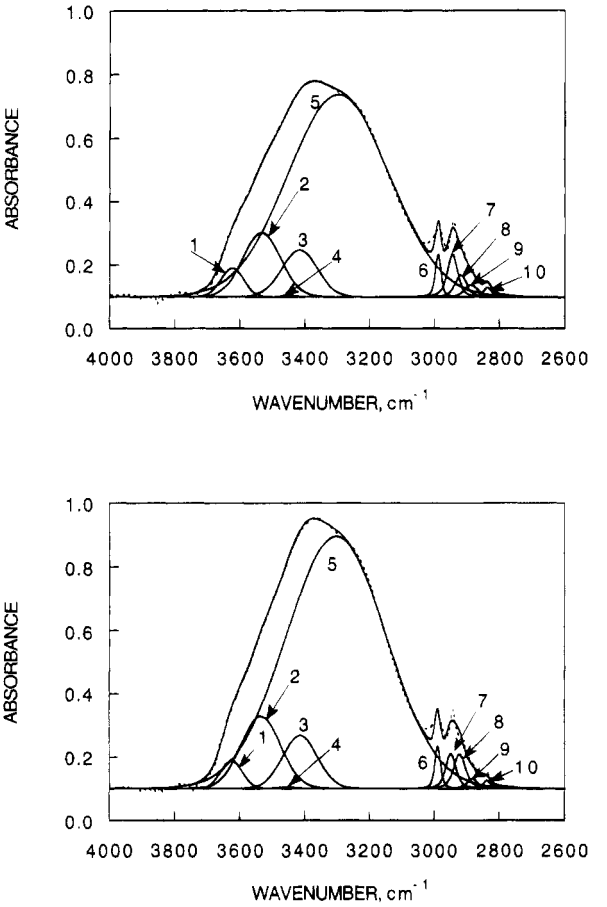

Figure 11. Spectral analysis for an annealed LB PMMA film with thickness of 0.1 μm after water contact at $t \cong 3$ s (top) and after equilibration with water at $t \cong 1$ h (bottom); unpolarized light was used; see Table 8 for curve fit parameters.

The relative areas of the hydrocarbon region were also compared at $t \approx 3$ s and at $t \approx 1$ h for both thin films (Tables 7 and 8). The changes of the relative areas on the hydrocarbon region for the thin spin cast film varied from 3 to −14% and for the LB film from −13 to −50%. The reason for this larger change was probably due to the poor fit on the hydrocarbon region due to the baseline noise. Nonetheless, these changes indicate that both films exhibited some microstructural changes upon contacting water.

Generally, the total integrated absorbance A^{I}_{tot} should be interpreted as the sum of two terms,

$$A^{I}_{tot} = A^{I}_{wo} + A^{I}_{ww} \tag{13}$$

where A^{I}_{wo} is the integrated absorbance of the water in

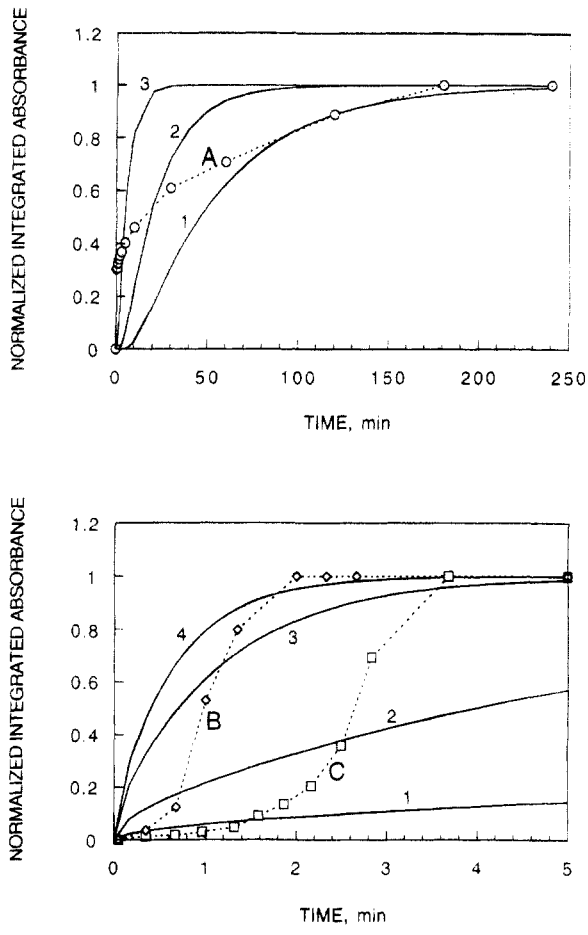

Figure 12. *Comparison of the water absorbance for thick spin* cast film (A, Figure 9) and thin films (B, spin cast; C, LB) to calculated absorbances based on eq 13. A one-dimensional Fickian diffusion model was used with an apparent diffusion coefficient, D_{app}, in cm^2/s: top, 4×10^{-11} (1), 10^{-10} (2), 5×10^{-10} (3), bottom, 10^{-15} (1), 10^{-14} (2), 5×10^{-14} (3), 10^{-13} (4).

the film initially, and A^I_{ww} is the absorbance of water on top of the film, expressed as follows:

$$A^I_{ww} = \varrho_{ww}\alpha_{ww}e^{-2\gamma_f l}\int_l^\infty e^{-2\gamma_w(x-l)}\,dx = \frac{\varrho_{ww}\alpha_{ww}}{2\gamma_w}e^{-2\gamma_f l} \quad (14)$$

For both the thick and the thin film in our experiments, $A^I_{wo} = 0$ because there was no water in the film initially.

Based on eqs 13 and 14, A^I_{tot} should be equal to zero ($A^I_{wo} = 6 \times 10^{-17}$ cm^{-1}) for the thick film ($l = 5.4$ μm). Then the first measurement (t $\geq$ 0 or ca. 3 s) implies that water had already entered the film in 3 s. Figure 12 (top) shows the jump between $t = 0$ s (calculated for the film before it contacted water) and the first measurement point at 3 s, for which the normalized absorbance was 0.3 (the integrated absorbance was 15.0 cm^{-1}). The fast initial penetration of the film by water was probably due to a significant volume fraction of defects, pinholes, or grain boundaries, which were filled fast, before the rest of the water diffused through the film. Subsequently, the rate of penetration decreased substantially with time. Similar results were reported for calcium stearate LB films.[26]

For the thin films, the normalization of the spectral intensity was done between the first measurement at 3 s and the last one (equilibrium) at 5 min. The water absorbance at the initial stages increased more slowly than for the thick films and followed different trends (Figure 12, bottom). Hence, these films were resistant to water uptake for a brief period (0.5–2 min), with this resistance being more pronounced for the LB film.

The initial absorbances (3 s) for the thin spin cast and the LB films were 317 and 307 cm^{-1}, respectively, whereas A^I_{tot} was calculated from eq 13 to be 197 cm^{-1}. This discrepancy is puzzling and cannot be due to error in the film thickness (which was established by profilometry). Probably the above equations, which were derived for systems consisting of nonabsorbing or weakly absorbing films and air ($k_3 = 0$) on top, are inaccurate for systems consisting of weakly absorbing films and strongly absorbing media, such as water ($k_3 = 0.3$). The observed discrepancy points the need for more rigorous models for the amplitude functions than those used here. Nonetheless, by normalizing the increases in water absorbances, the possible effects of strong absorption (k_3) should become minor and one can still track the dynamics of the water uptake in the film.

One interesting feature in Figure 12 is the similar water uptake rates (parallel lines B and C) of the thin LB and the spin cast films after the initial time lag. This result may indicate a similar diffusion mechanism for both thin films after the initial time delay. Since the densities of both films were found to be the same, the longer time delay observed in the LB film could be explained by a better alignment of the spread PMMA monolayers to form layers which are more dense, or have more hydrophobic surface, as also reported for PODMA [poly(octadecyl methacrylate)] monolayers.[35] A smaller water contact area, due to a less rough surface, and a more uniform penetration depth, as shown in Figure 1, may also increase this time delay for the LB film, as compared to the spin cast film.

The thin as well as the thick films absorbed a considerable amount of water. Their absorbances at long times increased by 60 cm^{-1} for the thin spin cast film, by 70 cm^{-1} for the LB film, and by 50 cm^{-1} for the thick spin cast film. The estimated water density for the thick film was 0.11 g/cm^3, from eq 12. The water densities in the thin films were 0.13 and 0.15 g/cm^3. For estimating the water density in these films, the absorptivities, α_{wf}, of both the thick and the thin films were taken to be equal to the value found from water, $\alpha_{ww} = 3.76 \times 10^7$ cm/g. This is a reasonable assumption, since bulk water dominates the permeation in these films upon contact with water. Since the sorbed water in the thick film was about 0.027 g per cm^3 of polymer, it follows that the rest of the water was bulklike, or that bulk water existed in pores or cavities in the film, or even that water was trapped in regions of imperfect adhesion between the film and the substrate. The water penetration experiment may, therefore, detect not only imperfections in the film microstructure but also imperfections in film deposition and film adherence to the substrate. In the thinner films a significant portion of the water detected may be due to water entering the space between the film and the ATR crystal, rather than the film structure. This would be consistent with the larger percentage of water detected in the thin films than in the thick film.

Relation of Water Uptake Dynamics to a Fickian Model. *This model was used to obtain some insight* into the water penetration and a first-order description of the process. If penetration followed a one-dimensional Fickian diffusion mechanism for the time-dependent water density in the film, $\varrho_{wf}(x,t)$, then the transient integrated absorbance $A^I_{tot}(t)$ would be

$$A^{I}_{tot}(t) = \alpha_{wf}\int_0^l \varrho_{wf}(x,t)e^{-2\gamma_f x}\,dx + \frac{\varrho_{ww}\alpha_{ww}}{2\gamma_w}e^{-2\gamma_f l} \quad (15)$$

where $\varrho_{wf}(x,t)$ would follow the unsteady diffusion equation $\partial\varrho_{wf}/\partial t = D\,\partial^2\varrho_{wf}/\partial x^2$, with the following initial and boundary conditions:

$$\varrho_{wf}(x,0) = 0; \quad \varrho_{wf}(l,t) = \varrho^{\infty}_{wf}; \quad \frac{\partial\varrho_{wf}}{\partial x}(0,t) = 0 \quad (16)$$

In this model, ϱ^{∞}_{wf} is the density of the water at the water/film interface and it is assumed to be equal to the final water density in the film after equilibration. The last boundary condition reflects the no-flux condition at the PMMA/crystal interface. The solution to such a transport problem is straightforward with the method of separation of variables:[36]

$$\varrho_{wf} = \varrho^{\infty}_{wf}\left[1 + \frac{4}{\pi}\sum_{n=1}^{\infty}\frac{(-1)^n}{2n-1}e^{-(2n-1)^2\pi^2(tD_{app}/l^2)/4} \times \cos\left[\frac{(2n-1)\pi}{2}\frac{x}{l}\right]\right] \quad (17)$$

By combining eqs 15 and 17, one obtains after analytical integration:

$$A^{I}_{tot}(t) = \frac{\varrho^{\infty}_{wf}\alpha_{wf}}{2\gamma_f}(1 - e^{-2\gamma_f l}) + \frac{4}{\pi}\varrho^{\infty}_{wf}\alpha_{wf} \times \left\{\sum_{n=1}^{\infty}\left[\frac{(-1)^n\left[2\gamma_f + (-1)^{n-1}e^{(-2\gamma_f l)}\frac{2n-1}{2l}\pi\right]e^{[-(2n-1)^2\pi^2 D_{app}(t/4l^2)]}}{(2n-1)\left(4\gamma_f^2 + (2n-1)^2\frac{\pi^2}{4l^2}\right)}\right]\right\} + \frac{\varrho_{ww}\alpha_{ww}}{2\gamma_w}e^{-2\gamma_f l} \quad (18)$$

Using eq 18, one can plot the normalized expected absorbance for various values of D_{app}, as shown in Figure 12, test whether the assumed mechanism is valid, and possibly estimate the range of D_{app}.

No single diffusivity value can fit the entire experimental curve, indicating that the mechanism is more complex than assumed in this model and that the film microstructure is not uniform. For the thick film, the data indicate a widely varying range of the effective diffusivities (the value that matches each data point with one model curve), from $D_{app} = 5 \times 10^{-10}$ to 4×10^{-11} cm^2/s. For the thin films, the data suggest a wider range of apparent diffusivities, between 10^{-13} and 10^{-15} cm^2/s. These results support the observation that the thin films are less permeable to water, probably because these films are more dense and have fewer pinhole defects that the thick film. These values should not be interpreted as molecular diffusivities but rather as averages of molecular diffusivities of different regions or related to dispersion coefficients through a complicated microporous structure. For better describing the observed transport, future work may consider more detailed microstructural information and more realistic penetration/diffusion mechanisms.

Conclusions

Spin coating and LB deposition can be used to produce fair-quality PMMA films. The LB method produces films of better thickness uniformity than the spin casting method. For thin films and better barrier properties, the LB method may have an edge. For thicker films, spin coating has the advantage of faster production but may need optimizing of the deposition conditions, to better control film quality. All films examined provide only short time barriers to water penetration.

The FTIR ATR technique was used for quantitatively interpreting the microstructural features of the films, for estimating the water content, and for probing the transport rate of water through the films. Spectral analysis of the polymer and the water bands was applied successfully to estimate changes in the dry and wet film microstructure after annealing and wetting treatments. No dramatic microstructural changes were detected for the dry and wet films examined in the present study. The thick (5.4 μm) spin cast film had considerably different molecular orientation and density than the thin (0.1 μm) spin cast film, as estimated from standard FTIR ATR theory. The molecular orientation and density, however, were identical for the thin films. These issues should be carefully considered in comparing mass transport properties of films of different thickness, even if produced by the same method.

PMMA absorbs a considerable amount of water, first in non-hydrogen-bonded water of hydration (or sorbed water) and then as bulklike water, in cracks and crevices and defects. The estimated density of all water absorbed by the annealed thick spin cast film was 0.11 g/cm^3. For the annealed thin spin cast film and LB film, it was 0.13 and 0.15 g/cm^3, respectively. Clearly the absorption depends on the deposition method and on the annealing procedure. The water transport and absorption results for nonannealed films were inconclusive because of film cracking.

Based on the above results, spin cast or LB films of atactic (uncross-linked) PMMA are poor barriers to water vapor and to liquid water. Contacting thick films with liquid water produces immediately fast water penetration, followed by slower transport. Equilibration took about 3 h for the 5.4 μm film, about 2 min for the 0.1 μm spin cast film, and about 4 min for the 0.1 μm LB film.

The overall water penetration was compared to a simple one-dimensional Fickian diffusion model. Not unexpectedly, the mechanism is clearly more complex than the model. Comparisons indicated effective diffusion coefficients between 5×10^{-10} and 4×10^{-11} cm^2/s for the thick spin cast film and between 10^{-13} and 10^{-15} cm^2/s for the thin films. The LB film, having a more hydrophobic and less rough film surface than the spin cast films, exhibited a 2 min time lag to transport of liquid water.

Acknowledgment. This work was supported in part by NSF (#CBT 864904, CTS 9004147, and CTS 9311159), and by a Purdue Research Foundation fellowship. We thank Professor Hilary S. Lackritz for helpful discussions.

Appendix

The thick nonannealed film was exposed under the same experimental conditions as the annealed films. No change was observed in the intensity of the ν C=O band when the film was exposed to water vapor. The density of the sorbed water at 89% relative humidity in the equilibrated bulk PMMA was estimated to be 0.019 g/cm^3 and the dichroic ratio of the ν C=O band remained

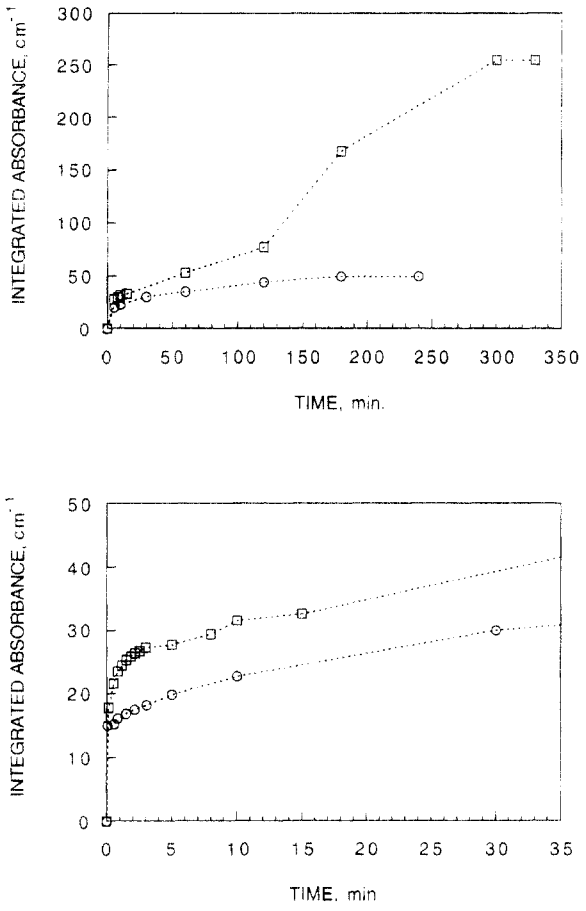

Figure A1. Integrated total water absorbance (in cm^{-1}) for nonannealed spin cast PMMA film (l = 5.7 μm) (□) and for annealed spin cast PMMA film (l = 5.4 μm) (○).

unchanged (0.77 ± 0.02), indicating no change in this group's molecular orientations. Also, there were probably more pinholes or film defects in this film. Annealing should diminish some of these film defects, as it causes the polymer to relax and consequently reduce its free volume. Figure A1 shows how the water absorbance of this film changes with time after contact with liquid water. The first measurement (3 s) was A^I = 17.8 cm^{-1}. After film saturation within 5 h, A^I was 250 cm^{-1}. The high intensity of the water band suggests that a significant portion of water penetrated the nonannealed film. Cracks were also observed in the film after water saturation. Most probably, the film cracked after about 150 min, as hinted by the substantial absorbance increase of the nonannealed film, compared to the annealed film. These cracks may occur because of uneven stresses in the polymer material as the solvent evaporates in the spin cast experiment. To minimize these stresses, which may increase as water absorbs, and to control the experiment better, it seems necessary to anneal the film above its glass transition temperature, as was done in all the other experiments reported here.

References and Notes

(1) Stroeve, P.; Franses, E. I.; Eds. *Molecular Engineering of Ultrathin Films*; Elsevier: London, 1987; also *Thin Solid Films* **1987**, *152*.
(2) Roberts, G. G.; Ed. *Langmuir-Blodgett Films*; Plenum Press: New York, 1990.
(3) Ulman, A. *An Introduction to Ultrathin Organic Films. From Langmuir-Blodgett to Self Assembly*; Academic Press: New York, 1991.
(4) Kuan, S. W. J.; Frank, C. W.; Fu, C. C.; Allee, D. R.; Maccagno, P.; Pease, R. F. W. *J. Vac. Sci. Technol.* **1988**, *B6*, 2274.
(5) Kuan, S. W. J.; Frank, C. W.; Yen Lee, Y. H.; Eimori, T.; Allee, D. R.; Pease, R. F. W.; Browning, R. *J. Vac. Sci. Technol.* **1989**, *B7*, 1745.
(6) Turner, D. T. *Polymer* **1982**, *23*, 197.
(7) Okamoto, K.-I.; Tanihara, N.; Watanabe, H.; Tanaka, K.; Kita, H.; Nakamura, A.; Kusuki, Y.; Nakagawa, K. *J. Polym. Sci.: Part B: Polym. Phys.* **1992**, *30*, 1223.
(8) Harrick, N. J. *Internal Reflection Spectroscopy*; John Wiley & Sons: New York, 1967.
(9) Zbinden, R. *Infrared Spectroscopy of High Polymers*; Academic Press: New York, 1964.
(10) Davydov, V. Ya.; Eremeeva, T. V.; Kiselev, A. V. *Kolloidn Zh.* **1981**, *43*, 144.
(11) Grinsted, R. A.; Clark, L.; Koenig, J. L. *Macromolecules* **1992**, *25*, 1235.
(12) Hartauer, K. J.; Martheson, L. E.; Guillory, J. K. *Appl. Spectrosc.* **1988**, *42*, 699.
(13) Mulder, M. *Basic Principles of Membrane Technology*; Kluwer Academic Publishers: London, 1991.
(14) Ahn, D. J.; Franses, E. I. *Thin Solid Films*, **1994**, *244*, 971.
(15) Robinson, R. A.; Stokes, R. H. *Electrolyte Solutions*, 2nd Ed.; Academic Press: New York, 1959.
(16) Bornside, D. E.; Macosko, C. W.; Scriven, L. E. *J. Electrochem. Soc.* **1991**, *138*, 317.
(17) Ahn, D. J.; Franses, E. I. *J. Phys. Chem.* **1992**, *96*, 9952.
(18) Haller, G. L.; Rice, R. W. *J. Phys. Chem.* **1970**, *74*, 4368.
(19) Harrick, N. J.; duPré, F. K. *Applied Optics* **1966**, *5*, 1739.
(20) Harrick, N. J.; Carlson, A. I. *Applied Optics* **1971**, *10*, 19.
(21) Graf, R. T.; Koenig, J. L.; Ishida, H. *Appl. Spectrosc.* **1985**, *39*, 405.
(22) Allara, D. L.; Baca, A.; Pryde, C. A. *Macromolecules* **1978**, *11*, 1215.
(23) Bertie, J. E.; Eysel, H. H. *Appl. Spectrosc.* **1985**, *39*, 392.
(24) Mirabella, F. M., Jr. *Appl. Spectrosc. Rev.* **1985**, *21*, 45.
(25) Ohta, K.; Iwamoto, R. *Appl. Spectrosc.* **1985**, *39*, 418.
(26) Marshbanks, T. L.; Ahn, D. J.; Franses, E. I. *Langmuir* **1994**, *10*, 276.
(27) Colthup, N. B.; Daly, L. H.; Wiberley, S. E. *Introduction to Infrared and Raman Spectroscopy*, 3rd ed.; Academic Press: New York, 1990.
(28) Brinkhuis, R. H. G.; Schouten, A. J. *Macromolecules* **1991**, *24*, 1496.
(29) Meloan, C. E. *Elementary Infrared Spectroscopy*; Macmillan: New York, 1963.
(30) Kajikawa, K.; Yamaguchi, T.; Anzai, T.; Takezoe, H.; Fukuda, A.; Okada, S.; Matsuda, H.; Nakanishi, H.; Abe, T.; Ito, H. *Langmuir* **1992**, *8*, 2764.
(31) Walrafen, G. E. In *Water, a Comprehensive Treatise*: *Vol 1: The Physics and Physical Chemistry of Water*; Franks, F., Ed.; Plenum Press: New York, 1972; p 202.
(32) Kesting, R. E. *Synthetic Polymeric Membranes*; McGraw-Hill: New York, 1971; p 230.
(33) Jain, K. J.; Varshney, M.; Maitra, A. *J. Phys. Chem.* **1989**, *93*, 7409.
(34) Christopher, D. J.; Yarwood, J.; Belton, P. S.; Hills, B. P. *J. Colloid Interface Sci.* **1992**, *152*, 465.
(35) Mumby, S. J.; Swalen, J. D.; Rabolt, J. F. *Macromolecules* **1986**, *19*, 1054.
(36) Crank, J. *The Mathematics of Diffusion*; Clarendon Press: Oxford, 1975.